4

Conductor-dominant transverse fields

In this chapter, we consider transverse field configurations that can be approximated as uniform along the z axis. We begin by considering the general form of the solutions to the magnetostatic equations in two dimensions. We next treat the fields produced by line currents, current sheets, and current blocks. We find that multipole errors are introduced when we approximate ideal current distributions with practical conductor configurations. The shapes of the fields discussed here are primarily determined by the location of the conductors. Any iron that may be present only acts to enhance the strength of the field in the magnet aperture. A high-field accelerator magnet is one example of a magnet that produces fields of this type. We conclude with a brief discussion of superconductors and 3D conductor configurations used at the end of these magnets.

4.1 General solution to the Laplace equation in two dimensions

The two-dimensional Laplace's equation in the polar coordinates r and θ is

$$\frac{1}{r}\,\partial_r(r\,\partial_r V) + \frac{1}{r^2}\,\partial_\theta^2\, V = 0. \tag{4.1}$$

This is identical with the first two terms in Equation 3.39, so the solutions for the radial and azimuthal dependence of the potential follow from Equations 3.43, 3.44, 3.46, and 3.47. Thus the general solution for Laplace's equation in polar coordinates has the form

$$V(r,\theta) = \sum_{n=1}^{\infty}(C_n r^n + D_n r^{-n})\,(E_n \cos\, n\theta + F_n \sin\, n\theta) + (C_0 \ln r + D_0)\;(E_0 + F_0). \tag{4.2}$$

https://doi.org/10.1017/9781009291156.005 Published online by Cambridge University Press

Example 4.1: vector potential inside a magnet aperture

The aperture of a magnet is the open area enclosed by the coils. We consider here the general form for the magnetic field in a magnet aperture. We use a polar coordinate system with the origin inside the aperture and let the variable V in Equation 4.2 refer to the z component of the vector potential. In addition, we assume that there are no external fields present outside the magnet and no current filaments inside the aperture. In this case, we can ignore the $n = 0$ terms in Equation 4.2. Since the potential must be finite at $r = 0$, we must have all the coefficients $D_n = 0$. Thus the vector potential inside the aperture has the form

$$A_z(r,\theta) = \sum_{n=1}^{\infty} C_n\, r^n (E_n \cos\, n\theta + F_n \sin\, n\theta). \tag{4.3}$$

The magnetic field is given by

$$\overrightarrow{B}(r,\theta) = \nabla \times \overrightarrow{A} = \hat{r}\,\frac{1}{r}\partial_\theta A_z - \hat{\theta}\,\partial_r A_z. \tag{4.4}$$

Evaluating the radial field component, we find

$$B_r(r,\theta) = \sum_{n=1}^{\infty} C_n\, r^{n-1}[-E_n\, n\sin\, n\theta + F_n\, n\cos\, n\theta]. \tag{4.5}$$

Defining the new coefficients

$$\begin{aligned} A_n &= -n\;\; C_n\, F_n \\ B_n &= -n\;\; C_n\, E_n, \end{aligned} \tag{4.6}$$

the radial field inside the magnet aperture can be written as

$$B_r(r,\theta) = \sum_{n=1}^{\infty} r^{n-1}(-A_n \cos\, n\theta + B_n \sin\, n\theta). \tag{4.7}$$

The coefficients A_n and B_n describe the multipole field content of the transverse field.[1] Returning to Equation 4.4, the azimuthal field component is

$$B_\theta(r,\theta) = -\sum_{n=1}^{\infty} C_n\, n\, r^{n-1}[E_n \cos\, n\theta + F_n \sin\, n\theta].$$

[1] *Caveat emptor*. The reader should be aware that a number of different definitions are used in the literature to describe the multipole content of a transverse field.

https://doi.org/10.1017/9781009291156.005 Published online by Cambridge University Press

Using Equation 4.6, the azimuthal field in the magnet aperture is

$$B_\theta(r,\theta) = \sum_{n=1}^{\infty} r^{n-1}(A_n \sin\, n\theta + B_n \cos\, n\theta). \tag{4.8}$$

On the midplane of the magnet ($\theta = 0$, $r = x$), B_x and B_y are given by power series in x

$$\begin{aligned} -B_x(x) &= -B_r(x,0) = A_1 + A_2 x + A_3 x^2 + \cdots \\ B_y(x) &= B_\theta(x,0) = B_1 + B_2 x + B_3 x^2 + \cdots . \end{aligned} \tag{4.9}$$

Example 4.2: scalar potential inside a magnet aperture
We again begin by considering the general form of the solution of Laplace's equation in polar coordinates given in Equation 4.2. We then specialize to the case for a region containing $r = 0$ and obtain an equation analogous to Equation 4.3.

$$\mu_0 V_m(r,\theta) = \sum_{n=1}^{\infty} G_n r^n (H_n \cos\, n\theta + I_n \sin\, n\theta). \tag{4.10}$$

The magnetic field is given by

$$\overrightarrow{B}(r,\theta) = -\mu_0 \nabla V_m = -\hat{r}\,\mu_0 \frac{\partial V_m}{\partial r} - \hat{\theta}\,\frac{\mu_0}{r}\,\frac{\partial V_m}{\partial \theta}.$$

Thus the radial field is

$$B_r = -\sum_{n=1}^{\infty} n\, G_n\, r^{n-1}(H_n \cos\, n\theta + I_n \sin\, n\theta). \tag{4.11}$$

The field components calculated from this potential must equal the same quantities calculated from the vector potential. We can make B_r have the same form as Equation 4.5 if we demand that

$$\begin{aligned} -n\, G_n H_n &= n\, C_n F_n = -A_n \\ -n\, G_n I_n &= -n\, C_n E_n = B_n. \end{aligned}$$

Thus we identify

$$\begin{aligned} G_n &= C_n \\ H_n &= -F_n \\ I_n &= E_n. \end{aligned}$$

https://doi.org/10.1017/9781009291156.005 Published online by Cambridge University Press

The scalar potential inside the aperture is then given by[2]

$$\mu_0 V_m(r,\theta) = \sum_{n=1}^{\infty} C_n\, r^n (E_n \sin n\theta - F_n \cos n\theta). \tag{4.12}$$

The resulting magnetic field components are still given by Equations 4.7 and 4.8.

If the field in some region is known, for example through calculations or measurements, then the multipole field coefficients can be determined using Fourier analysis. Multiplying both sides of Equation 4.8 by cos $m\theta$ and integrating around a circular path, we have

$$\int_0^{2\pi} B_\theta(r,\theta)\ \cos m\theta\, d\theta = \sum_{n=1}^{\infty} r^{n-1}[A_n\, \mathbb{I}_1 + B_n\, \mathbb{I}_2],$$

where for $m \geq 1$ and $n \geq 1$ the integrals have the values[3]

$$\mathbb{I}_1 = \int_0^{2\pi} \sin n\theta \cos m\theta\, d\theta = 0 \tag{4.13}$$

and

$$\begin{aligned} \mathbb{I}_2 &= \int_0^{2\pi} \cos n\theta \cos m\theta\, d\theta = \pi\, \delta_{mn} \\ &= \int_0^{2\pi} \sin n\theta \sin m\theta\, d\theta. \end{aligned} \tag{4.14}$$

Thus we find one set of multipole field components is given by

$$B_n = \frac{1}{\pi r^{n-1}} \int_0^{2\pi} B_\theta(r,\theta) \cos n\theta\, d\theta. \tag{4.15}$$

Likewise, we can multiply Equation 4.8 with sin $m\theta$ and find the other set of multipole components is

$$A_n = \frac{1}{\pi r^{n-1}} \int_0^{2\pi} B_\theta(r,\theta) \sin n\theta\, d\theta. \tag{4.16}$$

[2] We will see in the next chapter that this relationship between the vector and scalar potentials follows directly from the Cauchy-Riemann equations.
[3] CRC 497, 502.

https://doi.org/10.1017/9781009291156.005 Published online by Cambridge University Press

A similar analysis using Equation 4.7 for the radial component of the field gives

$$B_n = \frac{1}{\pi r^{n-1}} \int_0^{2\pi} B_r(r,\theta) \sin n\theta \, d\theta \tag{4.17}$$

and

$$A_n = \frac{-1}{\pi r^{n-1}} \int_0^{2\pi} B_r(r,\theta) \cos n\theta \, d\theta. \tag{4.18}$$

The strength of the multipole fields provides a measure of the field quality. Limits on the field uniformity are imposed by the application that needs the magnetic field. The presence of harmonics of the desired field limits the size of the useful magnet aperture. Sometimes, when examining the field quality of a magnet, it is more useful to examine the relative magnitude of the multipole coefficients with respect to the coefficient for the desired multipole. Thus for a dipole design, for example, one could calculate the dimensionless quantities

$$b_n = \frac{B_n \, r_0^{n-1}}{B_1},$$

where r_0 is a reference radius, typically ~2/3 of the magnet aperture.

The boundary conditions for the vector potential in polar coordinates at some radius r_b can be determined from the boundary conditions on the magnetic field. From the condition on the normal component of B, we have

$$B_r^{(1)} = B_r^{(2)}$$
$$\frac{1}{r_b} \frac{\partial A_z^{(1)}}{\partial \theta} = \frac{1}{r_b} \frac{\partial A_z^{(2)}}{\partial \theta}.$$

From this relation, we know that $A^{(2)}$ can differ from $A^{(1)}$ by at most a constant, which we can ignore since constants are removed when we take derivatives to obtain the field. Thus we have

$$A_z^{(2)}(r_b,\theta) = A_z^{(1)}(r_b,\theta). \tag{4.19}$$

From the boundary condition on H_t,

$$H_t^{(2)} - H_t^{(1)} = K,$$

we have

$$-\frac{1}{\mu^{(2)}} \frac{\partial A_z^{(2)}(r_b,\theta)}{\partial r} + \frac{1}{\mu^{(1)}} \frac{\partial A_z^{(1)}(r_b,\theta)}{\partial r} = K. \tag{4.20}$$

https://doi.org/10.1017/9781009291156.005 Published online by Cambridge University Press

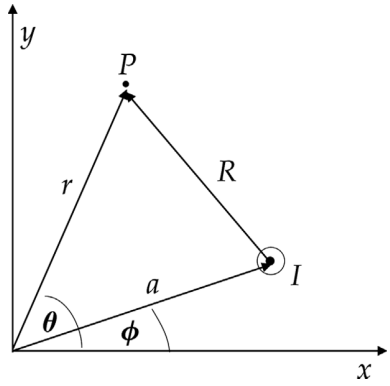

Figure 4.1 Geometry of a line current.

4.2 Harmonic expansion for a line current

Consider a line current perpendicular to the *x*-*y* plane, as shown in Figure 4.1. The vector potential for a line current was given in Equation 3.8

$$A_z(r,\theta) = -\frac{\mu I}{2\pi}\,\ln\left(\frac{R}{r_0}\right), \tag{4.21}$$

where the distance from the line current at $(a,\,\phi)$ to the observation point P located at $(r,\,\theta)$ is given by

$$R = \left\{(r\cos\theta - a\cos\phi)^2 + (r\sin\theta - a\sin\phi)^2\right\}^{1/2} \tag{4.22}$$

and r_0 is some constant reference radius for the two-dimensional potential. We look for a harmonic expansion for A_z. When $r > a$ we extract a factor of r^2 from the logarithm and find that

$$\ln(R) = \tfrac{1}{2}\,\ln(r^2) + \tfrac{1}{2}\,\ln\left[1 + \frac{a^2}{r^2} - 2\,\frac{a}{r}\,\cos\,(\theta-\phi)\right].$$

Writing the cosine in terms of complex exponentials gives

$$\begin{aligned}\ln(R) &= \ln(r) + \tfrac{1}{2}\ln\left[1 + \frac{a^2}{r^2} - \frac{a}{r}e^{i(\theta-\phi)} - \frac{a}{r}e^{-i(\theta-\phi)}\right]\\ &= \ln(r) + \tfrac{1}{2}\left[\ln\left(1 - \frac{a}{r}e^{i(\theta-\phi)}\right) + \ln\left(1 - \frac{a}{r}e^{-i(\theta-\phi)}\right)\right].\end{aligned}$$

https://doi.org/10.1017/9781009291156.005 Published online by Cambridge University Press

Using the series expansion for $\ln(1+x)$ for $x < 1$, we find

$$\ln(R) = \ln(r) - \frac{a}{r}\cos(\theta-\phi) - \frac{1}{2}\left(\frac{a}{r}\right)^2 \cos[2(\theta-\phi)] + \cdots$$
$$= \ln(r) - \sum_{n=1}^{\infty} \frac{1}{n}\left(\frac{a}{r}\right)^n \cos[n(\theta-\phi)].$$

Thus the vector potential for the line current when $r > a$ is [1]

$$A_z(r,\theta) = -\frac{\mu I}{2\pi}\ln(r) + \frac{\mu I}{2\pi}\sum_{n=1}^{\infty}\frac{1}{n}\left(\frac{a}{r}\right)^n \cos[n(\theta-\phi)] \tag{4.23}$$

plus a constant term involving r_0. The expansion of $\ln R$ for the case $r < a$ can be done in a similar manner by first extracting a factor of a^2 from the argument of the logarithm. This results in the vector potential

$$A_z(r,\theta) = -\frac{\mu I}{2\pi}\ln(a) + \frac{\mu I}{2\pi}\sum_{n=1}^{\infty}\frac{1}{n}\left(\frac{r}{a}\right)^n \cos[n(\theta-\phi)]. \tag{4.24}$$

Example 4.3: line current in circular iron cavity

Consider a line current at radius a inside the circular aperture of a piece of iron with radius R, as shown in Figure 4.2. We know from Equations 4.23 and 4.24 that the contribution to the total vector potential from the line current has different expansions depending on whether r is greater than or lesser than the radius a of the line current. Similarly, the field induced in the iron has different expressions depending on whether r is greater than or smaller than the radius R of the opening in the iron.[2, 3] The induced vector potential must have the general form given in Equation 4.2. To match the field from the line current at the boundaries, the induced field must have the same angular dependence as the line current. The induced field must also be finite at $r = 0$ and at $r \to \infty$. Let $k = I/2\pi$ and $\omega = \theta - \phi$. Then the total vector potential in the region (1) with $r < a$ is

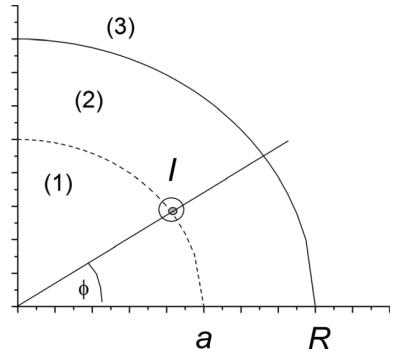

Figure 4.2 Quarter section of a line current in a circular iron cavity.

https://doi.org/10.1017/9781009291156.005 Published online by Cambridge University Press

$$A_{z1} = -\mu_0 k \ln(a) + \mu_0 k \sum_{n=1}^{\infty} \frac{1}{n} \left(\frac{r}{a}\right)^n \cos n\omega + \mu_0 \sum_{n=1}^{\infty} C_n r^n \cos n\omega.$$

In the region (2) with $a < r < R$ between the line current and the iron boundary, the vector potential is

$$A_{z2} = -\mu_0 k \ln(r) + \mu_0 k \sum_{n=1}^{\infty} \frac{1}{n} \left(\frac{a}{r}\right)^n \cos n\omega + \mu_0 \sum_{n=1}^{\infty} C_n r^n \cos n\omega.$$

Lastly, in the region (3) with $r > R$ inside the iron, the vector potential is

$$A_{z3} = -\mu k \ln(r) + \mu k \sum_{n=1}^{\infty} \frac{1}{n} \left(\frac{a}{r}\right)^n \cos n\omega + \mu \sum_{n=1}^{\infty} D_n r^{-n} \cos n\omega,$$

where $\mu = \mu_r \mu_0$ is the assumed constant permeability of the iron. We determine the unknown coefficients C_n and D_n by demanding continuity of

$$B_r = \frac{1}{r} \partial_\theta A_z$$

$$H_\theta = -\frac{1}{\mu} \partial_r A_z$$

at the surface $r = R$ of the iron.

$$\frac{\mu_0 k}{n} a^n R^{-n-1} + \mu_0 C_n R^{n-1} = \frac{\mu k}{n} a^n R^{-n-1} + \mu D_n R^{-n-1}$$

$$-C_n R^{n-1} = D_n R^{-n-1}.$$

This gives two equations in two unknowns, which can be solved to give,

$$C_n = \frac{k}{n} \frac{a^n}{R^{2n}} \frac{\mu - \mu_0}{\mu + \mu_0}$$

$$D_n = -\frac{k}{n} a^n \frac{\mu - \mu_0}{\mu + \mu_0}.$$

In the region inside the radius a of the line current, the vector potential can be expressed as

$$A_{z1} = -\frac{\mu_0 I}{2\pi} \ln(a) + \frac{\mu_0 I}{2\pi} \sum_{n=1}^{\infty} \frac{1}{n} \left(\frac{r}{a}\right)^n \left[1 + \alpha \left(\frac{a}{R}\right)^{2n}\right] \cos n\omega, \qquad (4.25)$$

https://doi.org/10.1017/9781009291156.005 Published online by Cambridge University Press

where

$$\alpha = \frac{\mu - \mu_0}{\mu + \mu_0}.$$

The term in brackets shows the enhancement factor due to the iron. For points inside the iron, the solution is

$$A_{z3} = \frac{\mu I}{2\pi}\left[-\ln(r) + \sum_{n=1}^{\infty}\frac{1}{n}\left(\frac{a}{r}\right)^n(1-\alpha)\cos n\omega\right]. \tag{4.26}$$

We are now in a position to relate the solution of the previous example with the method of images for a circular boundary that we discussed in Section 2.7. For the region interior to the filament, $r < a$, the vector potential can be written in the form

$$A_{z1} = -\frac{\mu_0 I}{2\pi}\ln(a) + \frac{\mu_0 I}{2\pi}\sum_{n=1}^{\infty}\frac{1}{n}\left(\frac{r}{a}\right)^n\cos n\omega + \frac{\mu_0 I}{2\pi}\sum_{n=1}^{\infty}\frac{1}{n}\, r^n\frac{\alpha}{r_1^n}\cos n\omega, \tag{4.27}$$

where

$$r_1 = \frac{R^2}{a}.$$

Comparing with Equation 4.24, the first two terms give the potential for the true line current at $r = a$. Since in magnetostatics constant terms in the potential have no physical effects, we can arbitrarily add to the potential a constant term

$$-\frac{\mu_0 I}{2\pi}\ln(r_1).$$

Then this term plus the last term in Equation 4.27 give the potential for a line current at r_1 with current αI. Thus the vector potential in region (1) can be written as

$$A_{z1} = A_{LC}(a) + \alpha A_{LC}(r_1),$$

where A_{LC} is the vector potential for a line current. For the region inside the iron, $r > R$, let us define

$$\beta = 1 - \alpha = \frac{2\mu_0}{\mu + \mu_0}.$$

Then Equation 4.26 can be rewritten in the form

$$A_{z3} = \frac{\mu I}{2\pi}\left[-\ln r + \beta\ \ln r - \beta\ \ln r + \beta\ \sum_{n=1}^{\infty}\frac{1}{n}\left(\frac{a}{r}\right)^n\cos n\omega\right].$$

https://doi.org/10.1017/9781009291156.005 Published online by Cambridge University Press

Using Equation 4.23 for the vector potential of a line current, we find

$$A_{z3} = \frac{\mu I}{2\pi}\left[-(1-\beta)\ \ln r + \beta\left(-\ln r + \sum_{n=1}^{\infty}\frac{1}{n}\left(\frac{a}{r}\right)^n \cos n\omega\right)\right]$$
$$= \alpha\, A_{LC}(0) + \beta\, A_{LC}(a).$$

We see that the coefficients α and β are the same as those for the image currents in Equations 2.27–2.30.

4.3 Field for a current sheet

Consider a conductor in the form of an infinitely thin sheet that is uniform in the z direction, as shown in Figure 4.3. Assume here that the current also flows in the z direction. From the Biot-Savart law for a current sheet, Equation 1.13, we have

$$\vec{B} = \frac{\mu_0}{4\pi}\int \frac{\vec{K}\times\vec{R}}{R^3}dS$$

Assume the observation point P is in the x-y plane, as shown in Figure 4.4. We have

$$\vec{K} = \frac{dI}{ds}\,\hat{z}$$
$$\rho^2 = r^2 + a^2 - 2\ r\,a\ \cos\,(\theta-\phi)$$
$$R^2 = \rho^2 + z^2$$
$$dS = ds\ dz,$$

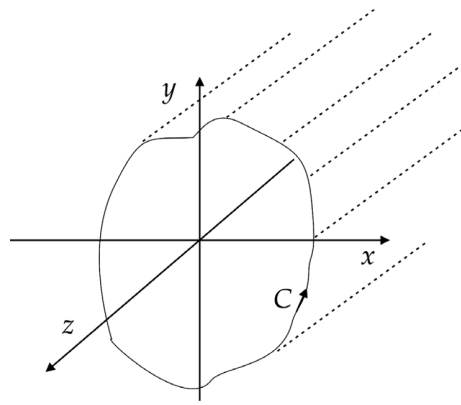

Figure 4.3 Current sheet with cross-section along the curve C and extending infinitely along the z direction.

https://doi.org/10.1017/9781009291156.005 Published online by Cambridge University Press

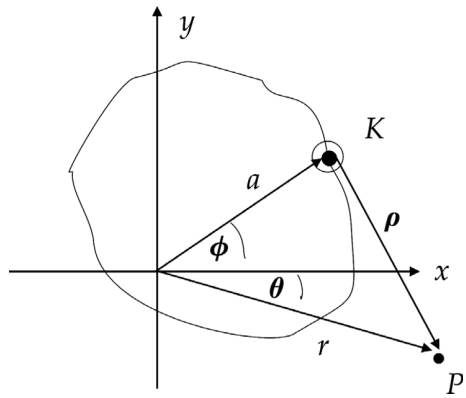

Figure 4.4 Sheet geometry.

where $a = a(s)$, $\phi = \phi(s)$ and s is the arclength around the sheet. The vector ρ is the distance between the current element and the field point in the x-y plane. Thus

$$\begin{aligned}\overrightarrow{B}(r,\theta) &= \frac{\mu_0}{4\pi}\int K(s)\int_{-\infty}^{\infty}\frac{\hat{z}\times(\overrightarrow{\rho}+z\,\hat{z})}{\{\rho^2+z^2\}^{3/2}}\,dz\,ds \\ &= \frac{\mu_0}{4\pi}\int K(s)\;\mathbb{I}(\rho)\;\hat{z}\times\overrightarrow{\rho}\;\;ds,\end{aligned}$$

where[4]

$$\mathbb{I}(\rho) = \int_{-\infty}^{\infty}\frac{dz}{\{\rho^2+z^2\}^{3/2}} = \frac{2}{\rho^2}. \tag{4.28}$$

Thus we find that the field from the current sheet is given by

$$\overrightarrow{B}(r,\theta) = \frac{\mu_0}{2\pi}\int K(s)\,\frac{\hat{z}\times\overrightarrow{\rho}}{\rho^2}\,ds. \tag{4.29}$$

It will also be useful to have an expression for the vector potential of a current sheet. Assuming the sheet is composed of parallel line currents and using Equation 4.21, we have

$$A_z(r,\theta) = -\frac{\mu_0}{2\pi}\int K(s)\ln\left(\frac{\rho}{\rho_0}\right)\,ds. \tag{4.30}$$

[4] GR 2.271.5.

https://doi.org/10.1017/9781009291156.005 Published online by Cambridge University Press

For the case of a circular sheet with constant radius a,

$$ds = a\, d\phi$$
$$K = \frac{dI}{d\phi}\,\frac{d\phi}{ds} = \frac{1}{a}\,\frac{dI}{d\phi}.$$

The field due to the circular sheet is

$$\overrightarrow{B}(r,\theta) = \frac{\mu_0}{2\pi}\int_{\phi_1}^{\phi_2} \frac{dI}{d\phi}\,\frac{\hat{z}\times\overrightarrow{\rho}}{\rho^2}\, d\phi \tag{4.31}$$

and the vector potential is

$$A_z(r,\theta) = -\frac{\mu_0}{2\pi}\int_{\phi_1}^{\phi_2} \frac{dI}{d\phi}\,\ln\left(\frac{\rho}{\rho_0}\right)\, d\phi. \tag{4.32}$$

Example 4.4: field between two parallel, straight current sheets
Consider the two parallel current sheets shown in Figure 4.5. The current, which is uniform along y, flows into the page on the sheet on the right and returns back out of the page on the sheet on the left. The field observation point P is at (x_o, y_o). We have

$$\overrightarrow{\rho} = (x_o - x)\,\hat{x} + (y_o - y)\,\hat{y}$$
$$K = \frac{dI}{dy}.$$

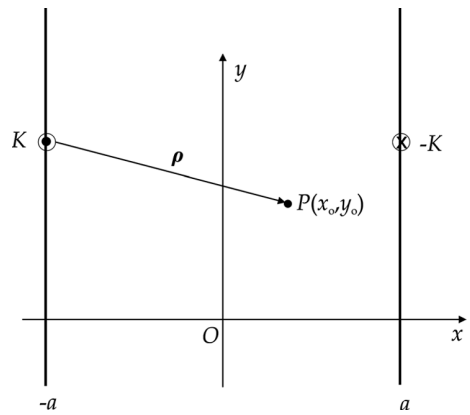

Figure 4.5 Parallel current sheets.

https://doi.org/10.1017/9781009291156.005 Published online by Cambridge University Press

Applying Equation 4.29, the field can be written as

$$\overrightarrow{B}(x_o, y_o) = \frac{\mu_0}{2\pi} K \int_{-\infty}^{\infty} \left[-\frac{(x_o - a)\hat{y} - (y_o - y)\hat{x}}{(x_o - a)^2 + (y_o - y)^2} + \frac{(x_o + a)\hat{y} - (y_o - y)\hat{x}}{(x_o + a)^2 + (y_o - y)^2} \right] dy.$$

All the current elements on both sheets give positive B_y because the magnitude of x_o is smaller than a. Thus we can write

$$B_y = \frac{\mu_0}{2\pi} K \ [(a - x_o) \ \mathbb{I}_1 + (a + x_o) \ \mathbb{I}_2],$$

where[5]

$$\mathbb{I}_1 = \int_{-\infty}^{\infty} \frac{dy}{(x_o - a)^2 + (y_o - y)^2} = \frac{\pi}{a - x_o}$$
$$\mathbb{I}_2 = \int_{-\infty}^{\infty} \frac{dy}{(x_o + a)^2 + (y_o - y)^2} = \frac{\pi}{a + x_o}.$$

Thus the vertical field between the sheets is

$$B_y = \mu_0 \frac{dI}{dy}. \tag{4.33}$$

This is, as expected, twice the field we found for a single sheet in Equation 1.17 and independent of the location of the observation point. In a similar manner, we find

$$B_x = \frac{\mu_0}{2\pi} K[y_o \mathbb{I}_1 - \mathbb{I}_3 - y_o \mathbb{I}_2 + \mathbb{I}_4],$$

where

$$\mathbb{I}_3 = \int_{-\infty}^{\infty} \frac{y}{(x_o - a)^2 + (y_o - y)^2} dy$$

and $\mathbb{I}_4$ is a similar integral with $x_o + a$ in the denominator. If we let D represent the denominator, then[6]

$$\mathbb{I}_3 = \tfrac{1}{2} \ln[D]_{-\infty}^{\infty} + y_o \mathbb{I}_1.$$

Using l'Hopital's rule, we can show that the first term vanishes, and find that

$$\mathbb{I}_3 = y_o \ \mathbb{I}_1$$
$$\mathbb{I}_4 = y_o \ \mathbb{I}_2.$$

[5] GR 2.172. [6] GR 2.175.1.

https://doi.org/10.1017/9781009291156.005 Published online by Cambridge University Press

Substituting back in, we find that the horizontal field between the sheets vanishes.

$$B_x = 0.$$

Thus there is a pure dipole field in the region between the current sheets.

4.4 Ideal multipole current sheet

Assume we have a circular current sheet with radius a and with azimuthal current density in the z direction given by

$$\frac{dI}{d\phi} = I_0 \cos m\phi,$$

where I_0 is the current flowing at the midplane ($\phi = 0$). We obtain the vector potential for the sheet by integrating the weighted distribution of the vector potential for a line current. Let us first consider the case where the observation point (r, θ) has $r < a$. Using Equation 4.24 for the line current and ignoring the constant term, the vector potential for the multipole sheet is

$$A_z = \frac{\mu I_0}{2\pi} \sum_{n=1}^{\infty} \frac{1}{n} \left(\frac{r}{a}\right)^n \int_0^{2\pi} \cos m\phi \ \cos\left[n(\theta - \phi)\right] d\phi.$$

Expanding the integrand and using Equations 4.13 and 4.14, the integral has the value

$$\int_0^{2\pi} \cos m\phi \ \cos\left[n(\theta - \phi)\right] d\phi = \begin{cases} 0 & \text{if } m \neq n \\ \pi \cos m\theta & \text{if } m = n \end{cases}. \tag{4.34}$$

Therefore the vector potential for $r < a$ is [4]

$$A_z(r, \theta) = \frac{\mu I_0}{2m} \left(\frac{r}{a}\right)^m \cos m\theta \tag{4.35}$$

and the components of the magnetic field are

$$\begin{aligned} B_r(r, \theta) &= -\frac{\mu I_0}{2a} \left(\frac{r}{a}\right)^{m-1} \sin m\theta \\ B_r(r, \theta) &= -\frac{\mu I_0}{2a} \left(\frac{r}{a}\right)^{m-1} \cos m\theta. \end{aligned} \tag{4.36}$$

https://doi.org/10.1017/9781009291156.005 Published online by Cambridge University Press

In the case of a dipole distribution ($m = 1$),

$$B_y = B_r \sin\theta + B_\theta \cos\theta = -\frac{\mu I_0}{2a}$$
$$B_x = B_r \cos\theta - B_\theta \sin\theta = 0$$

showing that the $\cos\theta$ angular distribution also produces a pure vertical field in the magnet aperture.

For the case when $r > a$, we use Equation 4.23 for the vector potential of the line current and obtain

$$A_z = -\frac{\mu I_0}{2\pi}\int_0^{2\pi} \cos m\phi \ \ln r \, d\phi + \frac{\mu I_0}{2\pi}\sum_{n=1}^{\infty}\frac{1}{n}\left(\frac{a}{r}\right)^n \int_0^{2\pi} \cos m\phi \ \cos\left[n(\theta-\phi)\right] d\phi.$$

The first integral vanishes over a complete circle and the second integral can again be evaluated using Equation 4.34. Thus the vector potential of the multipole sheet for the region $r > a$ is

$$A_z(r,\theta) = \frac{\mu I_0}{2m}\left(\frac{a}{r}\right)^m \cos m\theta \tag{4.37}$$

and the magnetic field is

$$\begin{aligned} B_r(r,\theta) &= -\frac{\mu I_0}{2}\frac{a^m}{r^{m+1}}\sin m\theta \\ B_r(r,\theta) &= \frac{\mu I_0}{2}\frac{a^m}{r^{m+1}}\cos m\theta. \end{aligned} \tag{4.38}$$

Example 4.5: $\cos m\theta$ sheet in circular iron cavity

Consider a circular $\cos m\theta$ sheet with radius a inside a symmetric circular iron cavity with radius R. We first solve the boundary value problem using vector potentials. There are two vector potentials for the sheet, depending on whether r is smaller than or greater than a, and two vector potentials for the image effects in the iron, depending on whether r is smaller than or greater than R. The angular dependence of the image effects must also use the cosine term in Equation 4.2 and only the m^{th} term in the summation in order to match the boundary conditions. This introduces two unknown coefficients, C and D, and requires that the total vector potential for the three regions be given as

$$A_{z1} = \frac{\mu_0 I_0}{2m}\left(\frac{r}{a}\right)^m \cos m\theta + C\, r^m \cos m\theta$$
$$A_{z2} = \frac{\mu_0 I_0}{2m}\left(\frac{a}{r}\right)^m \cos m\theta + C\, r^m \cos m\theta$$
$$A_{z3} = \frac{\mu I_0}{2m}\left(\frac{a}{r}\right)^m \cos m\theta + D\, r^{-m} \cos m\theta.$$

https://doi.org/10.1017/9781009291156.005 Published online by Cambridge University Press

To determine the values for C and D, we demand that B_r and H_θ are continuous across the iron boundary.

$$\frac{\mu_0 I_0}{2}\left(\frac{a}{R}\right)^m + C\,m\,R^m = \frac{\mu I_0}{2}\left(\frac{a}{R}\right)^m + D\,m\,R^{-m}$$
$$C\frac{R^m}{\mu_0} = -D\frac{R^{-m}}{\mu}.$$

Solving these two equations, we find that the unknown coefficients are

$$C = \frac{\mu_0 I_0}{2\,m\,R^m}\left(\frac{a}{R}\right)^m \frac{\mu-\mu_0}{\mu+\mu_0}$$
$$D = -\frac{\mu I_0}{2\,m\,R^{-m}}\left(\frac{a}{R}\right)^m \frac{\mu-\mu_0}{\mu+\mu_0}.$$

Using these values, the vector potential is now known in the three regions. The effect of the iron can be summarized by defining the iron enhancement factor

$$\alpha_m = 1 + \frac{\mu_r - 1}{\mu_r + 1}\left(\frac{a}{R}\right)^{2m}, \tag{4.39}$$

which agrees with the enhancement factor from Equation 4.25. We can write the vector potential inside the magnet aperture as

$$A_{z1}(r,\theta) = \frac{\mu_0 I_0}{2m}\left(\frac{r}{a}\right)^m \alpha_m \cos m\theta. \tag{4.40}$$

The corresponding field components inside the aperture are

$$\begin{aligned} B_r(r,\theta) &= -\frac{\mu_0 I_0}{2a}\left(\frac{r}{a}\right)^{m-1}\alpha_m \sin m\theta \\ B_r(r,\theta) &= -\frac{\mu_0 I_0}{2a}\left(\frac{r}{a}\right)^{m-1}\alpha_m \cos m\theta. \end{aligned} \tag{4.41}$$

The iron enhancement factor in Equation 4.39 ignores any saturation effects in the iron. When saturation becomes significant, the enhancement factor for the dipole field is decreased. In addition, the saturation of the iron does not occur uniformly. This causes changes in the field from the azimuthal distribution of the enhanced currents, leading to sextupole and higher multipole errors in the field in the magnet aperture. Fortunately, there are techniques, such as modifying the iron shape, which can be used to adjust the value of B_3 at a fixed operating current.[5]

https://doi.org/10.1017/9781009291156.005 Published online by Cambridge University Press

Example 4.6: cos $m\theta$ sheet in circular iron cavity using the scalar potential
It is instructive to use an alternative method of solving the preceding boundary value problem. In this case, we will use the scalar potential and take into account the presence of the current sheet through the addition of another pair of boundary conditions. Unlike the previous example, the unknown coefficients here take into account both the field from the sheet and the field from the images in the iron. We know from the boundary condition across a current sheet, Equation 2.23, that the angular dependence of the current must match the angular dependence of the fields on either side of the sheet. Since the fields are given by the derivative of the potential and the current goes like cos $m\theta$, this implies that we must use the sine term in Equation 4.2 for the potential. Thus the scalar potentials for the three regions are

$$\begin{aligned} V_{m1} &= A\, r^m \sin m\theta \\ V_{m2} &= (B\, r^m + C\, r^{-m})\ \sin m\theta \\ V_{m3} &= D\, r^{-m} \sin m\theta. \end{aligned}$$

The boundary conditions at the sheet are

$$\begin{aligned} A\ a^m &= B\, a^m - C\, a^{-m} \\ -m(B\, a^m + C\, a^{-m}) &+ m\, A\ a^m = I_0, \end{aligned}$$

while the boundary conditions at the iron surface are

$$\begin{aligned} -\mu_0(B\, R^m - C\, R^{-m}) &= \mu\, D\, R^{-m} \\ B\, R^m + C\, R^{-m} &= D\, R^{-m}. \end{aligned}$$

Solving the four equations for the four unknowns, we find

$$A = \frac{I_0}{2ma^m}\ \alpha_m$$

$$B = \frac{I_0\, a^m}{2mR^{2m}}\ \frac{\mu - \mu_0}{\mu + \mu_0}$$

$$C = -\frac{I_0\, a^m}{2m}$$

$$D = -\frac{\mu_0 I_0\, a^m}{m(\mu + \mu_0)}.$$

Evaluating the field components inside the magnet aperture, we again obtain Equation 4.41.

https://doi.org/10.1017/9781009291156.005 Published online by Cambridge University Press

4.5 Multipole dependence on the current distribution

We next seek to determine how the multipole fields in a magnet aperture are related to the current distribution on a circular current sheet.

Recall that the vector potential for a line current at (a, ϕ) is

$$A_z(r,\theta) = \frac{\mu I}{2\pi}\sum_{m=1}^{\infty}\frac{1}{m}\left(\frac{r}{a}\right)^m \cos\left[m(\theta-\phi)\right].$$

The corresponding azimuthal field component is

$$B_\theta(r,\theta) = -\frac{\mu I}{2\pi}\sum_{m=1}^{\infty}\frac{r^{m-1}}{a^m}\cos\left[m(\theta-\phi)\right]. \tag{4.42}$$

From Equation 4.15, the contribution to the normal multipole is

$$\begin{aligned} B_n &= \frac{1}{\pi r^{n-1}}\int_0^{2\pi} B_\theta(r,\theta)\cos n\theta\, d\theta \\ &= -\frac{\mu I}{2\pi^2}\sum_{m=1}^{\infty}\frac{1}{a^m}\int_0^{2\pi}\cos\left[m(\theta-\phi)\right]\cos n\theta\, d\theta . \end{aligned}$$

Expanding the cosine and integrating, we find

$$\begin{aligned} B_n &= -\frac{\mu I}{2\pi^2}\sum_{m=1}^{\infty}\frac{1}{a^m}\,\pi\cos m\phi\,\delta_{mn} \\ &= -\frac{\mu I}{2\pi a^n}\cos n\phi . \end{aligned} \tag{4.43}$$

For a current sheet, we can generalize this by integrating over the current distribution.

$$B_n = -\frac{\mu}{2\pi a^n}\int_0^{2\pi}\frac{dI}{d\phi}\cos n\phi\, d\phi. \tag{4.44}$$

We can find the skew multipoles in a similar manner using Equation 4.16.

$$A_n = -\frac{\mu}{2\pi a^n}\int_0^{2\pi}\frac{dI}{d\phi}\sin n\phi\, d\phi. \tag{4.45}$$

As the name suggests, a multipole field is characterized by the number of poles it has around the circumference of the sheet. Every magnet has an equal number of positive and negative poles. We use the index N to refer to the design number of pole

https://doi.org/10.1017/9781009291156.005 Published online by Cambridge University Press

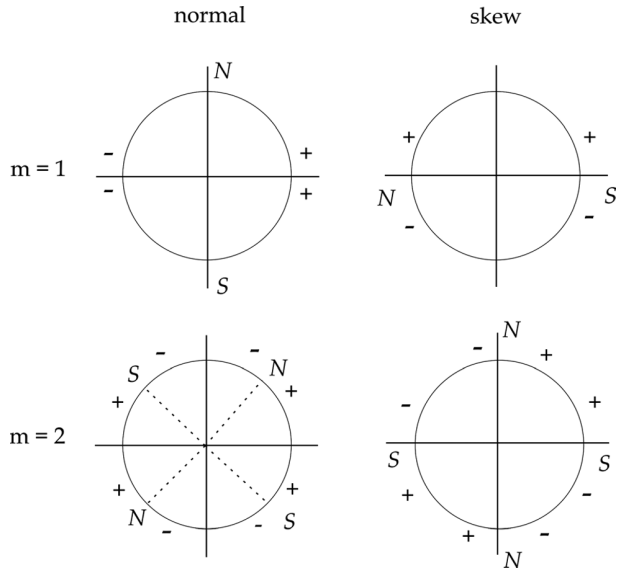

Figure 4.6 Multipole symmetries for dipoles ($m = 1$) and quadrupoles ($m = 2$). N and S indicate the north and south poles of the magnet. Plus and minus signs indicate the direction of the current.

pairs in the multipole magnet. Thus $N = 1$ refers to a dipole magnet because it has one pair of poles, $N = 2$ to a quadrupole, etc. The current in the magnet goes in opposite directions on the adjacent sides of a pole, as shown in Figure 4.6. This corresponds to the way these coils are usually wound, with the cable bending around the pole and returning in the opposite direction. As we can see from Equations 4.44 and 4.45, the multipole coefficients are weighted sums of the current distribution. The B_n coefficients are referred to as the *normal* multipoles. They are largest when the magnitude of the current reaches a maximum on the midplane. The A_n coefficients are referred to as the *skew* multipoles, which are largest when the current changes sign at the midplane. The field in a skew multipole of order N has the same pattern as the normal multipole rotated by $\pi/2N$. For example, a normal dipole has a vertical field, while a skew dipole has a horizontal field.

Consider the current distribution for an ideal multipole of order N given by

$$\frac{dI}{d\phi} = I_0 \cos N\phi.$$

The normal multipole coefficient for a complete angular distribution is

$$B_n = -\frac{\mu_0 I_0}{2\pi a^n} \int_{\phi_1}^{\phi_2} \cos N\phi \cos n\phi \, d\phi.$$

https://doi.org/10.1017/9781009291156.005 Published online by Cambridge University Press

From Equation 4.14, this vanishes unless $n = N$, in which case

$$B_N = -\frac{\mu_0 I_0}{2a^N}.$$

Similarly, Equation 4.13 shows that all the A_n coefficients vanish for this current distribution. The multipole coefficients are constructed such that they uniquely identify the symmetry of the current distribution. Likewise, an ideal current distribution of the form

$$\frac{dI}{d\phi} = I_0 \sin N\phi$$

is uniquely associated with the skew multipole A_N.

Example 4.7: quadrupole field
The coefficient for a quadrupole field corresponds to $N = 2$. The current density is given by

$$\frac{dI}{d\phi} = I_0 \cos 2\phi.$$

Thus

$$B_2 = -\frac{\mu_0 I_0}{2\pi\, a^2} \int_{\phi_1}^{\phi_2} \cos^2(2\phi)\, d\phi$$
$$= -\frac{\mu_0 I_0}{2\ a^2}.$$

4.6 Approximate multipole configurations

The idealized multipole current configurations discussed previously require a continuously varying distribution of current around the entire circumference. On the other hand, actual magnets are typically constructed from multiple layers of cables with uniform current density. Thus it is important to develop methods for approximating the desired multipole distribution, such that it produces the maximum amount of the desired multipole and still meets the required field quality for the magnet. To illustrate this, we consider here the design of a normal dipole magnet using circular current sheet sectors with constant current density. We know that the idealized current distribution for a dipole goes like $\cos\theta$. The simplest approximation to a $\cos\theta$ distribution is to put constant current sectors in each of the four quadrants, as shown in Figure 4.7. The multipole fields result from the sum of the contributions of the four sheets.

https://doi.org/10.1017/9781009291156.005 Published online by Cambridge University Press

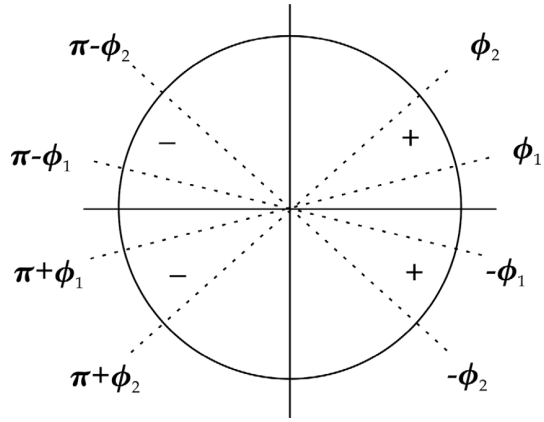

Figure 4.7 Dipole approximation.

$$B_n = -\frac{\mu_0 I}{2\pi a^n}\left\{\int_{\phi_1}^{\phi_2} \cos n\phi \, d\phi - \int_{\pi-\phi_2}^{\pi-\phi_1} \cdots - \int_{\pi+\phi_1}^{\pi+\phi_2} \cdots + \int_{-\phi_2}^{-\phi_1} \cdots\right\}$$

Let $S(\,) = \sin(\,)$. Then B_n can be written as the sum of eight sine terms.

$$\begin{aligned} B_n = -\frac{\mu_0 I}{2\pi n a^n} \, [\, & S(n\phi_2) - S(n\phi_1) - S(n\pi - n\phi_1) + S(n\pi - n\phi_2) \\ & -S(n\pi + n\phi_2) + S(n\pi + n\phi_1) - S(n\phi_1) + S(n\phi_2) \,]. \end{aligned}$$

If n is even, the terms in the brackets cancel, so $B_n = 0$. For odd values of n, we get

$$B_n = -\frac{2\mu_0 I}{\pi n a^n} \, [\sin n\phi_2 - \sin n\phi_1]. \tag{4.46}$$

A similar calculation shows that $A_n = 0$ for both odd and even values of n. Thus the allowed harmonics for this current configuration are just the B_n, for odd values of n.

In addition to the desired harmonic B_1 that represents the dipole, the approximation of the ideal multipole distribution above introduces other harmonics, which represent errors to the desired field. The dominant allowed error here is the sextupole term B_3. The angle ϕ_1 is typically set as close to 0 as possible in order to maximize the dipole strength. The angle ϕ_2 can then be used to remove the sextupole component from the field. Since

$$B_3 \simeq -\frac{2\mu_0 I}{3\pi a^3} \sin 3\phi_2,$$

we can eliminate the sextupole term by setting $\phi_2 = \pi/3$. Removing other allowed higher harmonics from the field requires additional degrees of freedom. A number

https://doi.org/10.1017/9781009291156.005 Published online by Cambridge University Press

of coil configurations have been proposed to approximate a cos θ distribution.[6] For example, a second current sector can be added in each quadrant that is separated from the first sector by a non-conducting spacer, or sectors could be added at different radii.[7] In principle, these additional sectors could also have independent currents. A two-layer design with spacers is described in Section 11.6.

The allowed harmonics for any multipole of order N follow from the requirement that the direction of the current is in opposite directions on either side of a pole. The first pole is located at

$$\phi = \frac{\pi}{2N}.$$

Referring to Figure 4.7, the current distributions on the opposite sides of the pole are

$$\frac{dI}{d\phi}(\beta) = -\frac{dI}{d\phi}(\phi),$$

where

$$\beta = 2\frac{\pi}{2N} - \phi = \frac{\pi}{N} - \phi.$$

To get a net contribution to a normal multipole of order n

$$B_n \propto \frac{dI}{d\phi}(\phi)\cos n\phi$$

from the current on both sides of the pole, the cosine function must also change sign.

$$\cos\left[n\left(\frac{\pi}{N} - \phi\right)\right] = -\cos n\phi$$

$$\cos\frac{n\pi}{N}\cos n\phi + \sin\frac{n\pi}{N}\sin n\phi = -\cos n\phi.$$

This requires that

$$\cos\frac{n\pi}{N} = -1$$

$$\sin\frac{n\pi}{N} = 0.$$

The sine equation requires that n/N is an integer, while the more restrictive cosine relation demands that n/N is an odd integer. Thus the allowed B_n must have

$$n = N(2m+1), \quad m = 0, 1, 2, \cdots \tag{4.47}$$

https://doi.org/10.1017/9781009291156.005 Published online by Cambridge University Press

Table 4.1 *Multipole symmetries [8]*

Symmetry	Normal multipoles	Skew multipoles	Example
Up-down symmetric		all $A_n = 0$	Normal dipole
Up-down antisymmetric	all $B_n = 0$		Skew dipole
Left-right symmetric	$B_n = 0$ for odd n	$A_n = 0$ for even n	Normal quadrupole
Left-right antisymmetric	$B_n = 0$ for even n	$A_n = 0$ for odd n	Normal dipole

A similar argument shows that the allowed skew multipoles also satisfy Equation 4.47.

The symmetry of the current distribution is directly related to the allowed harmonics. Let $K(\phi) = dI/d\phi$, for example, and assume the current distribution is up-down symmetric, so that

$$K(\phi) = K(-\phi).$$

Then the skew multipoles are

$$\begin{aligned} A_n &= -\frac{\mu_0}{2\pi a^n}\int_0^\pi [K(\phi)\sin n\phi + K(-\phi)\sin(-n\phi)]\,d\phi \\ &= \frac{\mu_0}{2\pi a^n}\int_0^\pi K(\phi)[\sin n\phi - \sin n\phi]\,d\phi = 0. \end{aligned}$$

Thus the fact that the dipole approximation had $A_n = 0$ follows from the up-down symmetry of the current distribution that we used. The consequences of some other symmetries for current distributions are listed in Table 4.1. These symmetries are inevitably violated to some extent in building an actual magnet and this leads to the presence of "nonallowed" multipoles in the fields. Random errors in the construction of the magnet can introduce values for any multipole.[9] If these nondesired multipoles exceed their tolerances, they must be removed by modifications in the manufacturing process or by introducing correction coils.

4.7 Field for a block conductor

Block conductors, which have a finite area in the x-y plane, are the most realistic approximation to actual conductors in two dimensions. We again consider the case where the conductor is infinitely long in the z direction and where the currents only flow along z. From the Biot-Savart law Equation 1.14, we have

$$\vec{B} = \frac{\mu_0}{4\pi}\int \frac{\vec{J}\times\vec{R}}{R^3}\,dV.$$

https://doi.org/10.1017/9781009291156.005 Published online by Cambridge University Press

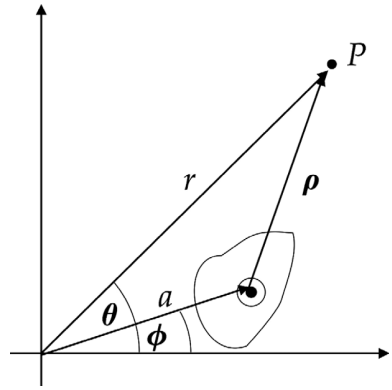

Figure 4.8 Current block geometry.

Assume an observation point P is located at (r, θ) in the x-y plane and the current element is at (a, ϕ), as shown in Figure 4.8. Let the vector ρ be the distance between the current element and the field point in the x-y plane and let σ be the current density in the conductor. Then we have

$$\begin{aligned} \overrightarrow{J} &= \sigma\, \hat{z} \\ \overrightarrow{R} &= \overrightarrow{\rho} + z\, \hat{z} \\ dV &= dS\ \ dz. \end{aligned}$$

Thus B can be written as

$$\begin{aligned} \overrightarrow{B}\,(r,\theta) &= \frac{\mu_0}{4\pi} \int \sigma \int_{-\infty}^{\infty} \frac{\hat{z} \times [\overrightarrow{\rho} + z\, \hat{z}]}{\{\rho^2 + z^2\}^{3/2}}\, dz\, dS \\ &= \frac{\mu_0}{4\pi} \int \sigma\, \mathbb{I}(\rho)\, \hat{z} \times \overrightarrow{\rho}\ dS, \end{aligned}$$

where $\mathbb{I}(\rho)$ is given by Equation 4.28. We find that the field from the current block is given by

$$\overrightarrow{B}\,(r,\theta) = \frac{\mu_0}{2\pi} \int \sigma\, \frac{\hat{z} \times \overrightarrow{\rho}}{\rho^2}\, dS. \tag{4.48}$$

The vector potential for a current block can be found by integrating the vector potential for the line current, Equation 4.21, over the area of the block.

$$A_z(r,\theta) = -\frac{\mu_0}{2\pi} \int \sigma \ln\left(\frac{\rho}{r_o}\right) dS. \tag{4.49}$$

https://doi.org/10.1017/9781009291156.005 Published online by Cambridge University Press

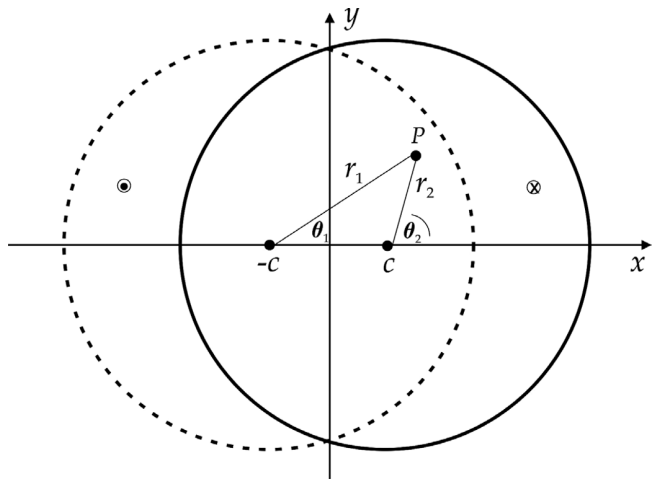

Figure 4.9 Overlapping circular cylindrical conductors.

Example 4.8: overlapping circular conductors
Imagine we have two circular cylindrical conductors with constant current density flowing in opposite directions. We know from Equation 1.27 that the field inside the conductor is

$$B_\phi = \frac{\mu_0 J \rho}{2}.$$

Suppose we overlap the two conductors with the centers displaced along the x axis at c and $-c$, as shown in Figure 4.9. The field at some arbitrary point P in the overlap region is the sum of the fields from the two conductors. From the geometry in the figure, we see that [10]

$$B_x = \frac{\mu_0 J}{2}[-r_2 \sin\theta_2 + r_1 \sin\theta_1] = 0$$

$$B_y = \frac{\mu_0 J}{2}[r_1 \cos\theta_1 - r_2 \cos\theta_2] = \frac{\mu_0 J}{2}\, 2c,$$

where $2c$ is the separation between the centers of the two circles. Thus the field in the overlap region is a pure dipole. The strength of the field is proportional to the separation between the circles. In the region where the two coils overlap, the net current is zero. Thus the conductor in the overlap region can be removed without affecting the field there.

Next we examine the coil thickness t as a function of the azimuthal angle ϕ, as shown in Figure 4.10. The coil thickness at some angle ϕ is the distance between the points P_1 and P_2. Point P_1 is determined by the intersection of circle 1

$$(x + c)^2 + y^2 = a^2$$

https://doi.org/10.1017/9781009291156.005 Published online by Cambridge University Press

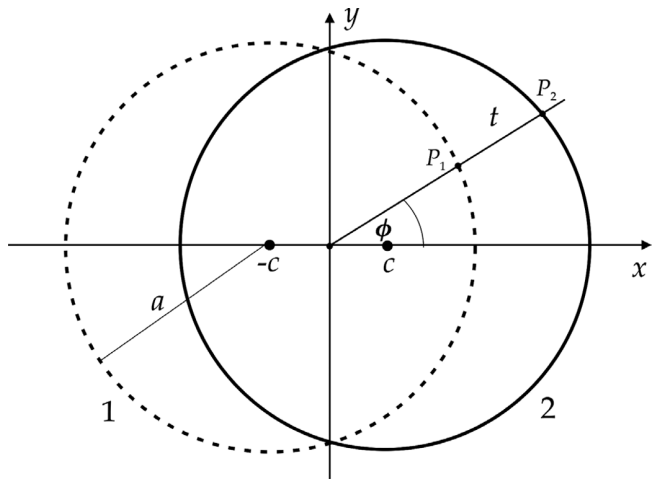

Figure 4.10 Conductor thickness for overlapping circle configuration.

with the straight line

$$y = x \tan \phi = mx.$$

We find that

$$x_1 = \frac{-c + \sqrt{a^2 - m^2c^2 + m^2a^2}}{1 + m^2}.$$

Point P_2 is determined by the intersection of circle 2

$$(x - c)^2 + y^2 = a^2$$

with the straight line. We find that the expression for x_2 is the same as the one for x_1, except that the first term in the numerator is $+c$ instead of $-c$. Thus we have

$$\Delta x = x_2 - x_1 = \frac{2c}{1 + \tan^2 \phi}$$
$$\Delta y = y_2 - y_1 = \Delta x \ \tan \phi.$$

The resulting thickness of the conductor is

$$t(\phi) = \sqrt{(\Delta x)^2 + (\Delta y)^2}$$
$$= 2c \cos \phi.$$

Thus the overlapping circular conductors represent another form of a cosine current distribution. Quadrupole fields can be designed in the same manner using overlapping elliptical conductors.[8]

https://doi.org/10.1017/9781009291156.005 Published online by Cambridge University Press

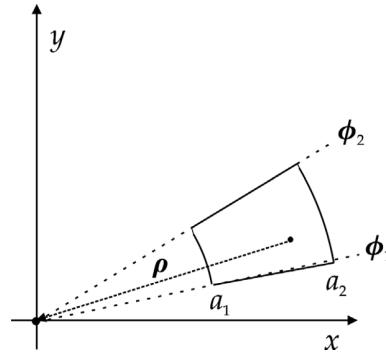

Figure 4.11 Annular current block.

Example 4.9: on-axis field of an annular sector with constant current density
Consider the annular sector conductor shown in Figure 4.11. For a field point on the axis we have

$$\overrightarrow{\rho} = -a\cos\phi\,\hat{x} - a\sin\phi\,\hat{y}.$$

Then Equation 4.48 gives

$$\overrightarrow{B}(0,0) = -\frac{\mu_0\sigma}{2\pi}\int_{a_1}^{a_2}\int_{\phi_1}^{\phi_2}\frac{\hat{z}\times(a\cos\phi\,\hat{x} + a\sin\phi\,\hat{y})}{a^2}\,a\,d\phi\,da$$

$$= -\frac{\mu_0\sigma}{2\pi}\int_{a_1}^{a_2}\int_{\phi_1}^{\phi_2}(\cos\phi\,\hat{y} - \sin\phi\,\hat{x})\;\;d\phi\,da.$$

Thus the on-axis field of the annular sector is

$$\overrightarrow{B}(0,0) = -\frac{\mu_0\sigma}{2\pi}(a_2 - a_1)[(\sin\phi_2 - \sin\phi_1)\hat{y} + (\cos\phi_2 - \cos\phi_1)\hat{x}]. \tag{4.50}$$

We see that the field for the case of constant current density is directly proportional to the radial thickness of the conductor.

Example 4.10: field due to a rectangular conductor
Consider a rectangular conductor with constant current density σ in the z direction, as shown in Figure 4.12. We substitute

$$\overrightarrow{\rho} = (x_o - x)\,\hat{x} + (y_o - y)\,\hat{y}$$

https://doi.org/10.1017/9781009291156.005 Published online by Cambridge University Press

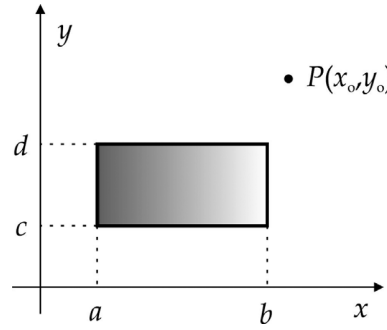

Figure 4.12 Rectangular conductor.

into Equation 4.48 and find that

$$\overrightarrow{dB} = \frac{\mu_0 \sigma}{2\pi} \frac{[(x_o - x)\,\hat{y} - (y_o - y)\,\hat{x}]}{(x_o - x)^2 + (y_o - y)^2} dS. \tag{4.51}$$

Looking at B_y, we have

$$B_y = \frac{\mu_0 \sigma}{2\pi} \int_a^b \int_c^d \frac{(x_o - x)}{(x_o - x)^2 + (y_o - y)^2}\, dx\, dy.$$

Integrating first over x, we evaluate[7]

$$\begin{aligned} \mathbb{I}_1(x_1, x_2) &= \int_{x_1}^{x_2} \frac{(x_o - x)}{(x_o - x)^2 + (y_o - y)^2}\, dx \\ &= -\frac{1}{2} \ln[(x_o - x)^2 + (y_o - y)^2]_{x_1}^{x_2}. \end{aligned}$$

Then integrating over y, we find[8]

$$\mathbb{I}_2(y_1, y_2, \alpha) = \int_{y_1}^{y_2} \ln[(x_o - \alpha)^2 + (y_o - y)^2]\, dy$$

$$= \left\{ -(y_o - y)\ln[(x_o - \alpha)^2 + (y_o - y)^2] + 2(y_o - y) - 2s(x_o - \alpha)\, \tan^{-1}\left[\frac{y_o - y}{s(x_o - \alpha)}\right] \right\}_{y_1}^{y_2},$$

where $s = \pm 1$. In order to get a physical solution, we need to choose $s = +1$ when $x_o > \alpha$ and $s = -1$ when $x_o < \alpha$. This is equivalent to taking the absolute value of $(x_o - \alpha)$. Thus we can write B_y as

[7] GR 2.175.1. [8] GR 2.733.1.

https://doi.org/10.1017/9781009291156.005 Published online by Cambridge University Press

$$B_y = -\frac{\mu_0\sigma}{4\pi}\left[\mathbb{I}_2(c,d,b) - \mathbb{I}_2(c,d,a)\right]$$

$$= -\frac{\mu_0\sigma}{4\pi}\Bigg\{ (y_o - c)\ \ln[(x_o-b)^2 + (y_o-c)^2] + 2|x_o - b|\ \tan^{-1}\left[\frac{y_o-c}{|x_o-b|}\right]$$

$$- (y_o - d)\ \ln[(x_o-b)^2 + (y_o-d)^2] - 2|x_o - b|\ \tan^{-1}\left[\frac{y_o-d}{|x_o-b|}\right]$$

$$- (y_o - c)\ \ln[(x_o-a)^2 + (y_o-c)^2] - 2|x_o - a|\ \tan^{-1}\left[\frac{y_o-c}{|x_o-a|}\right]$$

$$+ (y_o - d)\ \ln[(x_o-a)^2 + (y_o-d)^2] + 2|x_o - a|\ \tan^{-1}\left[\frac{y_o-d}{|x_o-a|}\right]\Bigg\}.$$

From the symmetry of Equation 4.51, we see that the result for B_x is the negative of the result for B_y with the substitutions

$$x \leftrightarrow y$$
$$x_o \leftrightarrow y_o$$
$$(a,b) \leftrightarrow (c,d).$$

Thus B_x is given by

$$B_x = \frac{\mu_0\sigma}{4\pi}\Bigg\{(x_o - a)\ \ln[(x_o-a)^2 + (y_o-d)^2] + 2|y_o - d|\ \tan^{-1}\left[\frac{x_o-a}{|y_o-d|}\right]$$

$$- (x_o - b)\ \ln[(x_o-b)^2 + (y_o-d)^2] - 2|y_o - d|\ \tan^{-1}\left[\frac{x_o-b}{|y_o-d|}\right]$$

$$- (x_o - a)\ \ln[(x_o-a)^2 + (y_o-c)^2] - 2|y_o - c|\ \tan^{-1}\left[\frac{x_o-a}{|y_o-c|}\right]$$

$$+ (x_o - b)\ \ln[(x_o-b)^2 + (y_o-c)^2] + 2|y_o - c|\ \tan^{-1}\left[\frac{x_o-b}{|y_o-c|}\right]\Bigg\}.$$

Using these expressions for the field, we show in Figure 4.13 a scan of the vertical field component along the x axis for a square conductor centered at the origin. The calculation using these equations fails when the observation point is located at one of the four corners of the rectangle.

We can find the multipoles produced by an annular sector conductor block analogously to the procedure used for current sheets in Section 4.5. The normal multipoles are given by

$$B_n = -\frac{\mu}{2\pi}\iint J(a,\phi)\ \frac{\cos n\phi}{a^{n-1}}\ da\ d\phi. \tag{4.52}$$

https://doi.org/10.1017/9781009291156.005 Published online by Cambridge University Press

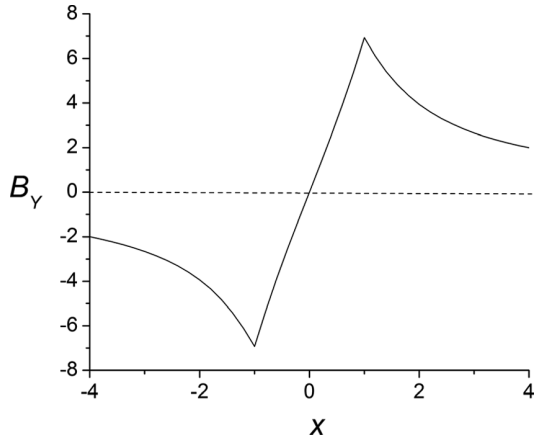

Figure 4.13 Vertical field from a square conductor with sides of length 2 centered at the origin.

The skew multipoles can be found in a similar manner and are given by

$$A_n = \frac{\mu}{2\pi}\iint J(a,\phi)\ \frac{\sin n\phi}{a^{n-1}}\ da\ d\phi. \tag{4.53}$$

4.8 Ideal multipole current block

Consider an annular current block with a pure multipole current density J. We assume that the block is composed of a radial distribution of ideal multipole current sheets extending from a_1 to a_2. We find the vector potential for the block by integrating the potential for a multipole sheet. The current density in the block is assumed to be proportional to cos $m\phi$.

There are three cases, depending on the radius of the field observation point r.

Case 1: $r < a_1$

The vector potential, Equation 4.35, for the ideal multipole sheet is

$$A_{zsh}(r,\theta) = \frac{\mu I_0}{2m}\left(\frac{r}{a}\right)^m \cos m\theta.$$

Then the vector potential for the current block is

$$A_z(r,\theta) = \frac{\mu J_0}{2m}\cos m\theta\int_{a_1}^{a_2}\left(\frac{r}{a}\right)^m a\ da.$$

https://doi.org/10.1017/9781009291156.005 Published online by Cambridge University Press

For $m \neq 2$, this can be written as

$$A_z(r,\theta) = \frac{\mu J_0}{2m}\, r^m \cos m\theta \left(\frac{a_2^{-m+2} - a_1^{-m+2}}{-m+2}\right). \tag{4.54}$$

When $m = 2$, we have

$$A_z = \frac{\mu J_0 r^2}{4} \cos 2\theta \ln\left(\frac{a_2}{a_1}\right). \tag{4.55}$$

Case 2: $r > a_2$

When the observation point is always larger than the radius of any of the multipole sheets, we use Equation 4.37 for the vector potential of the ideal multipole sheets.

$$A_{zsh}(r,\theta) = \frac{\mu I_0}{2m} \left(\frac{a}{r}\right)^m \cos m\theta.$$

The vector potential of the current block is

$$A_z(r,\theta) = \frac{\mu J_0}{2m\, r^m} \cos m\theta \int_{a_1}^{a_2} a^m\, a\, da.$$

Evaluating the integrals, we have

$$A_z(r,\theta) = \frac{\mu J_0}{2m}\, r^{-m} \cos m\theta \left(\frac{a_2^{m+2} - a_1^{m+2}}{m+2}\right). \tag{4.56}$$

Case 3: $a_1 < r < a_2$

In the third case, where the observation point can be inside the current block, we must break the radial integration into two parts, depending on the relative positions of r and the multipole sheet.

$$A_z(r,\theta) = \frac{\mu J_0}{2m} \cos m\theta \left[r^{-m} \int_{a_1}^{r} a^{m+1}\, da + r^m \int_r^{a_2} a^{-m+1}\, da\right].$$

Evaluating the integrals, we have for $m \neq 2$,

$$A_z = \frac{\mu J_0}{2m} \cos m\theta \left[r^{-m}\left(\frac{r^{m+2} - a_1^{m+2}}{m+2}\right) + r^m \left(\frac{a_2^{-m+2} - r^{-m+2}}{-m+2}\right)\right]. \tag{4.57}$$

For the case $m = 2$, we have instead

$$A_z = \frac{\mu J_0}{4} \cos 2\theta \left[r^{-2}\left(\frac{r^4 - a_1^4}{4}\right) + r^2 \ln\left(\frac{a_2}{r}\right)\right]. \tag{4.58}$$

https://doi.org/10.1017/9781009291156.005 Published online by Cambridge University Press

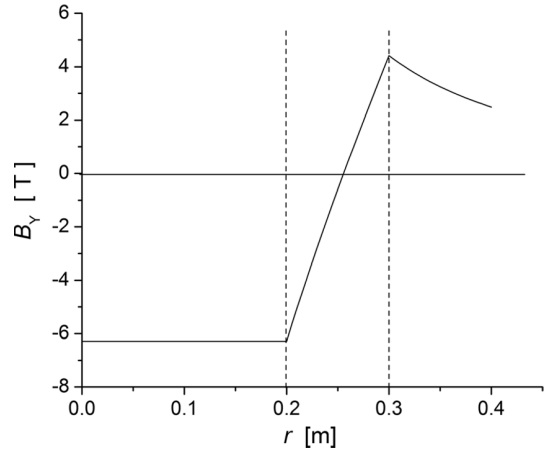

Figure 4.14 Radial scan of the vertical component of the magnetic field of an ideal dipole (m =1, a_1 = 0.2 m, a_2 = 0.3 m, J_0 = 100 A/mm^2).

The components of the magnetic field in each of these regions is easily computed from these vector potentials. Figure 4.14 shows a radial scan of the vertical component of the magnetic field along the midplane for an ideal dipole. The current block extends from 0.2 m to 0.3 m in this example. The field is constant and purely vertical inside the aperture, as expected. The field changes direction inside the current block. The strength of the field slowly falls off outside the block.

4.9 Field from a magnetized body

Let us consider the field intensity outside a magnetized body.[9] We saw from Equation 3.32 that the scalar potential for a magnetic body is

$$V_m = \frac{1}{4\pi} \int \frac{\overrightarrow{M'} \cdot \overrightarrow{R}}{R^3} dV'.$$

In the two-dimensional case, let us assume M only has x and y components. The scalar potential is

$$V_m = \frac{1}{4\pi} \int \left[M_x' \int_{-\infty}^{\infty} \frac{R_x}{R^3}\, dz' + M_y' \int_{-\infty}^{\infty} \frac{R_y}{R^3}\, dz' \right] dS',$$

[9] We will consider H inside a magnetized body in Chapter 9.

https://doi.org/10.1017/9781009291156.005 Published online by Cambridge University Press

where $R_x = x - x'$, etc. Define the transverse distance in the plane with $z = 0$ as

$$\overrightarrow{\rho} = R_x\,\hat{x} + R_y\,\hat{y}.$$

The integrals over z' are[10]

$$\int_{-\infty}^{\infty} \frac{R_x}{R^3}\,dz' = R_x \int_{-\infty}^{\infty} \frac{dz'}{\{\rho^2 + z'^2\}^{3/2}} = \frac{2R_x}{\rho^2}.$$

Then the two-dimensional potential is given by

$$V_m = \frac{1}{2\pi} \int \frac{\overrightarrow{M'} \cdot \overrightarrow{\rho}}{\rho^2}\,dS'. \tag{4.59}$$

The two-dimensional field is

$$\overrightarrow{H}_m = -\frac{1}{2\pi}\,\nabla \int \frac{\overrightarrow{M'} \cdot \overrightarrow{\rho}}{\rho^2}\,dS'.$$

Using the vector relation B.2,

$$\nabla\left(\overrightarrow{M'} \cdot \frac{\overrightarrow{\rho}}{\rho^2}\right) = \overrightarrow{M'} \times \left(\nabla \times \frac{\overrightarrow{\rho}}{\rho^2}\right) + \frac{\overrightarrow{\rho}}{\rho^2} \times \left(\nabla \times \overrightarrow{M'}\right) + \left(\overrightarrow{M'} \cdot \nabla\right)\frac{\overrightarrow{\rho}}{\rho^2} + \left(\frac{\overrightarrow{\rho}}{\rho^2} \cdot \nabla\right)\overrightarrow{M'}. \tag{4.60}$$

The gradient operator only acts on unprimed coordinates, so the second and fourth terms on the right-hand side vanish.

In the first term, we have using Equation B.6

$$\nabla \times \frac{\overrightarrow{\rho}}{\rho^2} = \frac{1}{\rho^2}\,\nabla \times \overrightarrow{\rho} + \nabla\left(\frac{1}{\rho^2}\right) \times \overrightarrow{\rho}. \tag{4.61}$$

The first term here vanishes because ρ is radial and so its curl vanishes. In the second term

$$\begin{aligned}\nabla\left(\frac{1}{\rho^2}\right) &= \hat{x}\,\partial_x\left(\frac{1}{\rho^2}\right) + \hat{y}\,\partial_y\left(\frac{1}{\rho^2}\right) \\ &= -\frac{2}{\rho^4}\,\overrightarrow{\rho}.\end{aligned}$$

Thus the cross-product of the last two factors in Equation 4.61 is 0, and the second term also vanishes.

[10] GR 2.271.5.

https://doi.org/10.1017/9781009291156.005 Published online by Cambridge University Press

Thus only the third term in Equation 4.60 survives and we have

$$\vec{H}_m = -\frac{1}{2\pi}\int (\vec{M'}\cdot\nabla)\frac{\vec{\rho}}{\rho^2}\, dS'. \tag{4.62}$$

Expanding the dot product,

$$\vec{H}_m = -\frac{1}{2\pi}\int \left[M_x'\,\partial_x\left(\frac{\vec{\rho}}{\rho^2}\right) + M_y'\,\partial_y\left(\frac{\vec{\rho}}{\rho^2}\right)\right] dS'.$$

Writing out the vector ρ in terms of its x and y components, taking the derivatives, combining terms, and dropping the primes, we find that the two-dimensional field from an iron element is given by

$$\vec{H}_m = -\frac{1}{2\pi}\int \left[\frac{\vec{M}}{\rho^2} - \frac{2(\vec{M}\cdot\vec{\rho})}{\rho^4}\,\vec{\rho}\right] dS. \tag{4.63}$$

4.10 Superconductors

High-field magnets are usually energized using superconducting cables. In the superconducting state, the resistivity vanishes, so a large current can flow through the magnet coils without losing power due to Joule heating. In a superconducting material, attractive forces between pairs of electrons are transmitted through vibrations in the material lattice.[11] The operating conditions for superconductivity lie below the surface of a three-dimensional space of temperature, magnetic field, and current density. The limiting values on each of the three axes are called the *critical* values. When the superconductor is not in the superconducting state, it is said to be in the *normal* state. There are several classes of superconducting materials. Type I materials exhibit the *Meissner effect*, where any external magnetic field is excluded from the interior of the superconductor. A magnetization is generated in the superconductor that just cancels the external field. This remains true as the external field is increased until it reaches the critical field H_c. Type I superconductors are perfect diamagnetic materials.

Some alloys of intermetallic compounds form what are called type II superconductors. Two important examples are NbTi and Nb_3Sn. The critical current density for these materials at 4 K is shown as a function of the magnetic flux density in Figure 4.15.[12] NbTi is a useful material for fields up to ~9 T at 4 K, whereas Nb_3Sn can be used up to ~22 T. These materials have two critical magnetic fields, H_{c1} and H_{c2}, which can be much larger than H_{c1}. For $H < H_{c1}$, the material

https://doi.org/10.1017/9781009291156.005 Published online by Cambridge University Press

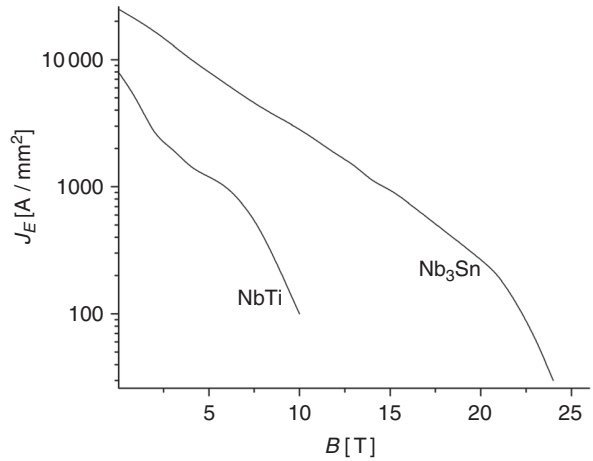

Figure 4.15 Engineering current density at 4 K as a function of the magnetic field.

completely excludes the external flux and it behaves like a type I superconductor. For $H_{c1} < H < H_{c2}$, flux begins to penetrate into the material and the magnitude of the magnetization begins to fall, but electrically it still has zero resistivity. The magnetic flux enters the superconductor in the form of discrete, quantized flux lines known as *fluxoids*. The field still vanishes in the material surrounding the fluxoids. The fluxoids can move because of Lorentz forces, creating heat. To stop the fluxoids from moving, inhomogeneities known as *pinning centers* must be introduced into the lattice. Finally when $H > H_{c2}$, the material returns to the normal state.

Magnets with superconducting cables must deal with the problem of *persistent currents*.[13] As the current in the magnet is ramped up or down, eddy currents[11] are induced in the superconductor. These induced shielding currents produce a field that opposes the change in the field caused by the magnet's power supply. Because of the lack of resistance in a superconductor, the decay times for the induced currents are very long. The persistent currents produce undesired sextupole and higher multipoles that can be particularly significant at low field values.

4.11 End fields

Although this chapter has mainly been concerned with transverse fields that are uniform along the z direction, real currents exist as closed loops, so we must comment on what happens at the end of this type of magnet. At the ends of a dipole, the conductor on one side of a pole must bend in such a way that it returns

[11] Eddy currents will be discussed in more detail in Section 10.4.

https://doi.org/10.1017/9781009291156.005 Published online by Cambridge University Press

in the opposite direction at the symmetrical location on the other side of the pole. There are several standard end configurations. If the aperture in the end regions does not need to be open, the simplest configuration is the *racetrack* coil.[10] The coil bends around an arc, maintaining the same vertical position as the coils in the straight part of the magnet. The *bedstead* end bends the conductors by 90° as quickly as possible and then crosses over the pole at a fixed z location. This configuration does keep a clear aperture in the end regions, but the sharp bend in the conductor may not be acceptable for mechanical reasons. Another type of end that maintains a clear aperture is the *saddle* end.[10] In this case, the conductor turns cross over the pole following an arc that is spread out over z. The magnetic design of real coil ends is usually done numerically using the Biot-Savart equation.

The end turns introduce additional multipole contributions to the field of a magnet. However, it is possible to define a new set of multipole coefficients defined in terms of the field components integrated along the axis of the magnet. Flux theorems have been developed that can relate these integrated multipoles to the geometry of the end turns.[14] The z locations where the cross-over for various conductors begin can be adjusted using spacers to help balance the integrated multipoles in the magnet.[15]

References

[1] W. Smythe, *Static and Dynamic Electricity*, 2nd ed., McGraw-Hill, 1950, p. 65.
[2] R. Gupta, *Field Calculations and Computations*, School at Centre for Advanced Technology, Indore, India, 1998, p. 32.
[3] N. Schwerg & C. Vollinger, Analytic models for the calculation of the iron yoke contribution in superconducting accelerator magnets, CERN Accelerator Technology Department report CERN/AT 2007-33, 2007.
[4] P. Schmuser, Superconducting magnets for particle accelerators, in M. Month & M. Dienes (eds.), *The Physics of Particle Accelerators*, AIP Conf. Proc. 249, vol. 2, 1992, p. 1106.
[5] G. Morgan, Shaping of magnetic fields in beam transport magnets, in M. Month & M. Dienes (eds.), *The Physics of Particle Accelerators*, AIP Conf. Proc. 249, vol. 2, 1992, p. 1256–1259.
[6] M. Wilson, *Superconducting Magnets*, Oxford University Press, 1983, p. 32.
[7] J. Coupland, Dipole, quadrupole and higher order fields from simple coils, *Nuc. Instr. Meth.* 78:181, 1970.
[8] A. Jain, Basic theory of magnets, in S. Turner (ed.), *CERN Accelerator School on Measurement and Alignment of Accelerator and Detector Magnets*, CERN 98–05, 1998, p. 25.
[9] G. Parzen, Random errors in the magnetic field of superconducting dipoles and quadrupoles, *Part. Acc.* 6:237, 1975.
[10] M. Wilson, *op. cit.*, p. 27–28.
[11] Ibid., p. 279.
[12] https://nationalmaglab.org/magnet-development/applied-superconductivity-center.

[13] P. Schmuser, *op. cit.*, p. 1123–1141.
[14] F. Mills & G. Morgan, A flux theorem for the design of magnet coil ends, *Part. Acc.* 5:227, 1973.
[15] R. Palmer & A. Tollestrup, Superconducting magnet technology for accelerators, in J. Jackson, H. Gove & R. Schwitters (eds.), *Annual Review of Nuclear and Particle Physics*, vol. 34, Annual Reviews Inc., 1984, p. 269–270.